HAL
open science

Metamagnetic transitions in Y0.5Er0.5Fe2D4.2 deuteride studied by high magnetic field and neutron diffraction experiments

V. Paul-Boncour, O. Isnard, M. Guillot, A. Hoser

To cite this version:

V. Paul-Boncour, O. Isnard, M. Guillot, A. Hoser. Metamagnetic transitions in Y0.5Er0.5Fe2D4.2 deuteride studied by high magnetic field and neutron diffraction experiments. Journal of Magnetism and Magnetic Materials, 2019, 477, pp.356-365. 10.1016/j.jmmm.2019.01.056 . hal-02056115

HAL Id: hal-02056115

https://hal.science/hal-02056115v1

Submitted on 13 Mar 2019

HAL is a multi-disciplinary open access archive for the deposit and dissemination of scientific research documents, whether they are published or not. The documents may come from teaching and research institutions in France or abroad, or from public or private research centers.

L'archive ouverte pluridisciplinaire **HAL**, est destinée au dépôt et à la diffusion de documents scientifiques de niveau recherche, publiés ou non, émanant des établissements d'enseignement et de recherche français ou étrangers, des laboratoires publics ou privés.

Metamagnetic transitions in $Y_{0.5}Er_{0.5}Fe_2D_{4.2}$ deuteride studied by high magnetic field and neutron diffraction experiments

V. Paul-Boncour[a*], O. Isnard[b,c], M. Guillot[d], A. Hoser[e]

[a]*Université Paris-Est, ICMPE (UMR7182), CNRS, UPEC, F-94320 Thiais, France*
[b]*CNRS, Institut Néel, 25 rue des Martyrs, BP 166X, F-38042 Grenoble, France*
[c]*Univ. Grenoble Alpes, Inst. Néel, F-38042 Grenoble, France*
[d]*LNCMI, CNRS, BP166, 38042 Grenoble Cedex 9, France*
[e] Helmholtz Zentrum Berlin, *Glienicker Str. 100, D-141 09 Berlin, Germany*

* Corresponding author, email: paulbon@icmpe.cnrs.fr

Abstract

The structural and magnetic properties of $Y_{0.5}Er_{0.5}Fe_2D_{4.2}$ deuteride have been investigated by continuous high field magnetic measurements up to 35 T and neutron powder diffraction experiments versus temperature and applied field. $Y_{0.5}Er_{0.5}Fe_2D_{4.2}$ crystallizes in a monoclinic structure (*Pc* space group) resulting from the deuterium order into 18 interstitial tetrahedral sites. At low field, the deuteride is ferrimagnetic (Ferri) up to 38 K, between 38 and 50 K, it undergoes a first order transition towards an antiferromagnetic (AFM) structure, which remains present up to T_N=115 K. Upon applied field, two different types of metamagnetic behavior are observed depending on the temperature range. Below 38 K, a forced ferrimagnetic-ferromagnetic (FM) transition is observed at a transition field B_{Trans} of only 7 T (at 2 K), which is among the smallest encountered for Fe rich intermetallics. B_{Trans} is not very sensitive to temperature changes nor to the Er content and its moderate value is explained by a deuterium induced weakening of the Er-Fe interaction. The second metamagnetic transition, observed between 38 and 150 K, from an AFM (Para) towards a FM structure, is related to the itinerant electron metamagnetic behavior of the Fe sublattice. B_{Trans} increases linearly versus temperature with a dB/dT slope of 0.24±0.01 T.K^{-1}. Above B_{Trans}, Er moments parallel to the Fe moments are induced.

Keywords: Laves phase compound; deuteride; neutron diffraction; high magnetic field; Metamagnetic transitions

1. Introduction

Rare-earth (*RE*) and 3d transition metal (*TM*) intermetallic compounds present a wide range of interesting fundamental magnetic properties and they can be used in many various applications (permanent magnets, magnetic storage, magnetic refrigeration…) related to the coupling between the localized magnetism of the 4f electrons and the itinerant behavior of 3d bands. The direct 3d-3d interactions are larger than the 4f-4f and 4f-3d indirect interactions (RKKY interactions), but the last one is responsible for the nature of the coupling between the *RE* and *TM* moments. The sign of the 4f-3d interaction in the ground state depends on the nature of the rare earth: it is positive for light rare-earths (*RE*=Ce-Eu) and negative for heavy rare-earth (*RE*=Gd-Tm). As a consequence, *RE-TM* intermetallic compounds with heavy rare-earth show an antiparallel coupling of the *RE* and *TM* moments in the ground state at low field and low temperature. A forced ferromagnetic alignment of the heavy *RE* moments with Fe or Co moments can be induced by the application of a high magnetic field. Such transitions have been studied in $RE_2Fe_{14}B$ (*RE*= Tm and Er) [1, 2], $ErFe_{11}Ti$ [3] single crystals, RE_2TM_{17} intermetallics (*RE*= Er, Tm; *TM*=Fe, Co) [4-6] using pulsed-field induction magnetometer. In Tm_2Co_{17} a ferromagnetic state with Tm and Co moments parallel to the *c*-axis was observed above 50 T and with a transition field B_{trans} of 39 T [4]. In Tm_2Fe_{17}, two step-like transitions were observed at 41 and 54 T but the ferromagnetic alignment was far from being reached at 60 T [6]. Hydrogen absorption has been used to decrease the transition magnetic field and even reach saturation. For example, a ferromagnetic state has been reached at only 57 T in $Tm_2Fe_{17}H_5$ [7]. Indeed, H insertion induces a large cell volume increase and consequently a reduction of the *RE-TM* interactions and a lowering of B_{trans}. In $TmFe_2H_{3.4}$ a spin reorientation has been observed with $B_{trans}\approx$ 10 T at 4.2 K, but the ferromagnetic state was reached at a saturation field B_{Sat} =100 T due to large Tm anisotropy [8]. In [7], a linear decrease of the reduced exchange integral $J_{RE\text{-}Fe}$ versus the relative cell volume change ($\Delta V/V$) was presented for selected RE_2Fe_{17} hydrides, deuterides, carbides and nitrides and $REFe_2$ hydrides. This decrease was found larger for the $REFe_2H_y$ Laves phase compounds which can absorb a significantly higher H content versus metal atom (H/M=1.1 for y=3.4) compared to $RE_2Fe_{17}H_y$ hydrides (H/M= 0.26 for y =5). Few results were reported for Er-Fe and Er-Co compounds (Er_2Co_{17}) but saturation could not be reached even at maximum applied fields [3, 5].

We have recently observed a forced ferromagnetic transition in $Y_{0.7}Er_{0.3}Fe_2D_{4.2}$ at a B_{trans} of only 8T below 30 K [9], which is even smaller than for $TmFe_2D_{3.4}$ (B_{trans} =10 T) [8]. At 4.2 K and using continuous high magnetic field up to 35 T (isothermal conditions) the saturation

magnetization reaches 6.3 μ_B (f.u.)$^{-1}$, close to the value expected for a ferromagnetic structure with parallel Fe and Er moments (6.5 μ_B).

At higher temperature $Y_{0.7}Er_{0.3}Fe_2D_{4.2}$ displays a second metamagnetic transition which has been related to the itinerant electron metamagnetic (IEM) behavior of the Fe sublattice. At low field $Y_{0.7}Er_{0.3}Fe_2D_{4.2}$ undergoes a ferromagnetic–antiferromagnetic (FM-AFM) transition at T_{M0} = 66 K. Above T_{M0}, a field induced AFM-FM transition is observed, with a linear increase of B_{Trans} versus applied field. As the Er moments order below T_{Er}= 55 K (B=0), the Er sublattice should be paramagnetic above T_{M0}. However, the increase of the magnetization curves above B_{Trans} cannot be only explained by the sum of the ferromagnetic contribution of the Fe sublattice and the paramagnetic contribution of the Er atoms. To explain this observation, it has been assumed that Er moments parallel to the Fe moments are also induced above B_{Trans}.

The first aim of this study is therefore to investigate the nature and the mechanism of the forced ferri-ferromagnetic transition, which was observed at low temperature in $Y_{0.7}Er_{0.3}Fe_2D_{4.2}$, by studying a compound with larger Er content. The second goal it is to observe more clearly the influence of the Er content on the FM-AFM transition and understand the behavior of the Er sublattice under applied field above T_{M0}.

For this purpose, we have investigated the structural and magnetic properties of $Y_{0.5}Er_{0.5}Fe_2D_{4.2}$ deuteride using both high magnetic field measurements up to 35 T in isothermal conditions and neutron powder diffraction under applied field at different temperatures. These results will be presented and compared with those of $Y_{1-x}Er_xFe_2D_{4.2}$ deuterides (x = 0, 0.3). A more general discussion will be performed about forced ferromagnetic transitions and IEM behavior in comparison with other *RE*-Fe(Co) systems displaying similar type of transition and discuss the influence of hydrogen insertion.

2. Experimental methods

The synthesis methods of the $Y_{0.5}Er_{0.5}Fe_2$ intermetallic compound and corresponding deuterides are described in details in refs. [9, 10]. Two deuteride samples have been prepared by a Sievert method: a first one with a small mass of m=0.5 g (S1) and the second one with larger mass m=11.2 g for neutron diffraction experiments (S2). Both samples were quenched into liquid nitrogen after deuterium absorption to avoid deuterium release and slowly heated under air up to room temperature in order to passivize the surface and avoid further deuterium

desorption. The average D content determined from volumetric method and change of mass after absorption was 4.25±0.10 D f.u^{-1}.

The crystal structure of intermetallic and both deuterides was checked by powder X-ray diffraction (XRD) at room temperature on a D8 Bruker diffractometer (Cu K_α radiation). $Y_{0.5}Er_{0.5}Fe_2$ was found to crystallize in the cubic C15 structure (*Fd-3m* space group) with *a*= 7.3182(1) Å (*V*=391.93 Å^3). The electron probe microanalysis (EPMA) confirms that this compound is single phase with an average composition $Y_{0.52(6)}Er_{0.48(6)}Fe_{2.10(7)}$ calculated over 200 points.

The magnetization measurements were performed using a conventional Physical Properties Measurement System (PPMS-9T) from Quantum Design operating with field up to 9 T. Additional high field magnetic measurements were performed in Grenoble High Magnetic Field Laboratory (GHMFL, Grenoble, France) in high continuous magnetic field up to 35 T. The experimental procedures of the magnetic studies are detailed in [11]. Isothermal variations $M_T(B)$ were then obtained. It is noted that after sweeping the field up and down at a given temperature the absence of remanent magnetization was checked before increasing temperature.

Neutron powder diffraction (NPD) patterns of $Y_{0.5}Er_{0.5}Fe_2D_{4.2}$ have been registered at 300 K on the high-resolution spectrometer *3T2* in the Laboratoire Léon Brillouin (LLB, CEA, Saclay, France) with a wavelength of 1.225 Å. Additional NPD measurements were performed with the *D1B* instrument at the Institut Laue Langevin (ILL, Grenoble, France) with temperature varying from 2 to 300 K. On the *D1B* instrument the diffraction patterns have been recorded over an angular range of 80° (2θ) starting at 3° and using a multidetector with a step width of 0.2° between each of the 400 ^{3}He detection cells. In this configuration *D1B* is operating with a wavelength of λ = 2.52 Å selected by a (002) Bragg reflection of a pyrolytic graphite monochromator, the take-off angle being 44.2° in 2θ. Due to the high flux available on the instrument, temperature evolution of the diffraction pattern has been recorded *in situ* during heating by recording the diffraction patterns every 3 K. The powder sample was introduced in vanadium cylindrical sample container.

NPD measurements have been also performed between 2 and 170 K in vertical magnetic field up to 10 T on E6 focusing diffractometer in Helmholtz Zentrum Berlin (HZB, Berlin, Germany). The powder sample introduced in an aluminum cylindrical sample container was frozen using deuterated alcohol to avoid preferred orientation of grains with the magnetic field.

The selected wavelength was 2.454 Å. The angular range was between 3 ° < 2θ < 113 ° with a step width of 0.15 °.

All the XRD and NPD patterns were analysed using the Rietveld refinement method implemented in the Fullprof code [12].

3. Experimental Results

3.1 Crystal structure

The XRD analysis of $Y_{0.5}Er_{0.5}Fe_2D_{4.2}$ S1 and S2 samples at room temperature (RT) shows that the main phase has a monoclinic structure isostructural to that of $YFe_2D_{4.2}$. The S1 sample was found single phase compound, but the second S2 sample contained two additional cubic phases with smaller cell volume, corresponding to deuteride phases with smaller D content. The XRD results are reported in Table 1. The monoclinic cell is described in the *Pc* space group that has been previously determined by NPD measurements to fully describe the crystal structure of $YFe_2D_{4.2}$ taking into account the ordering of deuterium atoms [13]. This monoclinic structure corresponds to a distortion of the cubic structure of the pristine compound with a mean cell volume increase $\Delta V/V$= 26.8% for $Y_{0.5}Er_{0.5}Fe_2D_{4.2}$.

The NPD pattern of S2 sample measured at 300 K on 3T2 was refined with the same monoclinic structure than $YFe_2D_{4.2}$ and $Y_{0.7}Er_{0.3}Fe_2D_{4.2}$ in *Pc* space group [9, 13] and two cubic phases with *Fd*-3*m* space group. The results of the refinement are given in Table 2 and the refined NPD pattern is presented in Fig. 1. The monoclinic *b* cell parameter has a particular behavior compared to the two other *a* and *c* parameters: it is expanded while the two others are contracted and it is doubled along the *b* axis compared to the values obtained by symmetry lowering starting from a cubic structure with the same cell volume expansion. The *a*, *b*, *c* and *V* cell parameters of the monoclinic structure in $Y_{0.5}Er_{0.5}Fe_2D_{4.2}$ are smaller than that of $YFe_2D_{4.2}$ as expected from the smaller radius of Er relative to Y. The monoclinic cell volume was reduced of 1.26 % compared to $YFe_2D_{4.2}$. The monoclinic angle β remains similar in both compounds. In the monoclinic phase there are 4 *RE* sites (with 0.5 Y and 0.5 Er on each RE site), 8 Fe sites and 18 deuterium sites. The deuterium atoms are located in 15 RE_2Fe_2 and 3 $REFe_3$ (D11, D17 and D18) tetrahedral interstitial sites with occupancy factors ranging between 0.62 and 1. No D atom were observed in Fe4 sites which have smaller size. The total D content 4.04 D (f.u.)$^{-1}$ is smaller than that refined for $YFe_2D_{4.2}$ but comparable to that of $Y_{0.7}Er_{0.3}Fe_2D_{4.2}$ (4.05 D (f.u.)$^{-1}$). As in this monoclinic structure they are 96 available RE_2Fe_2 and 32 $REFe_3$

tetrahedral interstitial sites, this means that 81 RE_2Fe_2 and 29 $REFe_3$ remain empty. The existence of empty sites is partially explained by the repulsion between two D atoms closer than 2 Å. The lowering of symmetry in a monoclinic structure results from a minimization of the total energy compared to a disordered cubic structure and leads also to a displacement of the metal atoms to accommodate the presence of interstitial deuterium atoms. Some Fe-Fe interatomic distances are elongated whereas other are shortened.

The cell volumes of the two cubic phases in sample S2 are smaller than the monoclinic one and the number of D atoms located in RE_2Fe_2 sites smaller than in the monoclinic phase. This indicates a partial deuterium desorption from this sample despite our trial to avoid it.

Table 1: Cell parameters of $YFe_2D_{4.2}$ and $Y_{0.5}Er_{0.5}Fe_2D_{4.2}$ deuterides S1 and S2 at 293 K.

Compounds	S.G.	*a* (Å)	*b* (Å)	*c* (Å)	*β* (°)	*V* (Å^3)	Wt %
$YFe_2D_{4.2}$	*Pc*	5.507(1)	11.472(2)	9.428(1)	122.354(1)	502.96(9)	100
$Y_{0.5}Er_{0.5}Fe_2D_{4.2}$ S1	*Pc*	5.4825(2)	11.4286(4)	9.3894(3)	122.359(2)	496.94(2)	100
$Y_{0.5}Er_{0.5}Fe_2D_{4.2}$ S2	*Pc*	5.4875(3)	11.4126(6)	9.3943(4)	122.429(2)	496.57(2)	77(1)
	Fd-3m	7.9028(7)				493.57(8)	17(1)
	Fd-3m	7.5757(4)				434.77(4)	6(1)

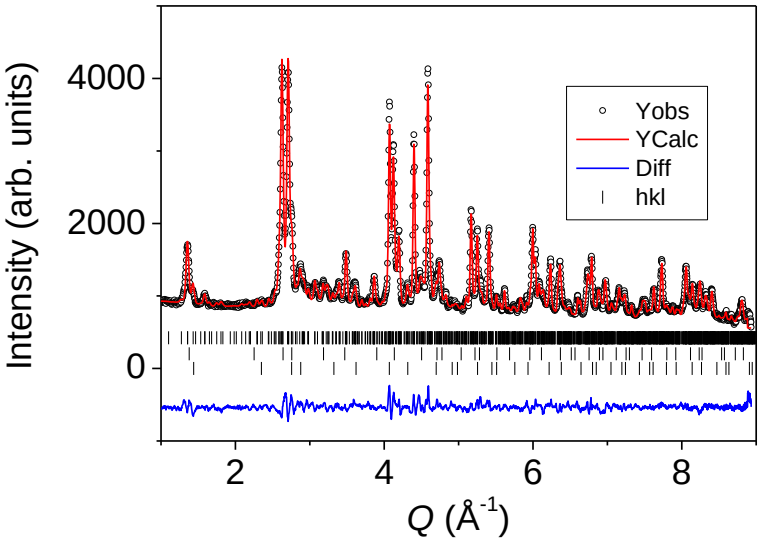

Fig. 1: Refined NPD pattern of $Y_{0.5}Er_{0.5}Fe_2D_{4.2}$ (sample S2) measured in 3T2 at 300 K (λ= 1.225 Å). Refinement with one monoclinic and two cubic phases. (Q = 4π sinΘ /λ).

Table 2: Results of the refinement of $Y_{0.5}Er_{0.5}Fe_2D_{4.2}$ NPD pattern measured on 3T2 at 300 K. The Debye Waller factors were constrained to the same values for Y/Er, Fe and D atoms respectively. The Y and Er atoms were located on the same sites with an occupancy ratio 0.5:0.5 in agreement with the chemical analysis.

Atom	*x*	*y*	*z*	*B* (Å^2)	N_{occ}
Y1, Er1	0.140	0.119	0.869	0.83(5)	1
Y2, Er2	0.873	0.372	0.636		1
Y3, Er3	0.112	0.375	0.362		1
Y4, Er4	0.880	0.121	0.132		1
Fe1	0.492	0.127	0.488	0.77(3)	1
Fe2	0.029	0.128	0.515		1
Fe3	0.503	0.243	0.256		1
Fe4	0.505	0.244	0.751		1
Fe5	0.008	0.374	-0.005		1
Fe6	0.494	0.494	0.240		1
Fe7	0.479	0.992	0.737		1
Fe8	0.508	0.382	0.001		1
D1	0.553(15)	0.618(5)	0.846(8)	1.58(11)	0.71(9)
D2	0.446(15)	0.628(4)	0.134(6)		0.77(9)
D3	0.497(11)	0.137(5)	0.154(7)		0.62(10)
D4	0.868(8)	0.274(3)	0.826(5)		1.00(8)
D5	0.133(9)	0.004(3)	0.635(4)		1.00(8)
D6	0.118(8)	0.277(4)	0.155(5)		0.97(10)
D7	0.175(8)	0.777(4)	0.168(5)		1.00(9)
D8	0.872(9)	0.467(4)	0.840 (5)		0.97(9)
D9	0.871(7)	0.975(4)	0.838(5)		1.00(9)
D10	0.279 (10)	0.466(4)	0.807(5)		0.81(9)
D11	0.647(8)	0.135(3)	0.721(4)		0.96(9)
D12	0.772(9)	0.740(3)	0.786(5)		0.74(8)
D13	0.563(7)	0.237(3)	0.939(4)		1.00(8)
D14	0.169(8)	0.838 (3)	0.904(4)		1.00(9)
D15	0.826(8)	0.567(3)	0.596(5)		0.82(9)
D16	0.499(7)	0.974(3)	0.427(4)		1.00(8)
D17	0.291(10)	0.525(4)	0.531(5)		0.79(9)
D18	0.732(8)	0.193(3)	0.466(4)		0.91(8)
	Space group	Cell parameters	*V* (Å^3)	D/f.u.	wt%
Mono	*P* 1 *C* 1	*a*=5.4822(2) Å *b*=11.4136(5) Å *c*=9.3839(3) Å *β*=122.424(3)°	495.63 (3)	4.04(4)	79.3(1.5)
Cub 1	*Fd-3m*	*a*= 7.8939(6) Å	491.90 (7)	3.2(2)	17.2(8)
Cub 2	*Fd-3m*	*a*= 7.5642(8) Å	432.81(8)	1.6(4)	3.5(4)
	R_{Bragg} :5.7%	Rp: 10%	Rwp: 10.3 %	Chi2: 6.5	

3.2 Magnetic properties

3.2.1 Magnetic measurements

The magnetic properties of the two S1 and S2 samples are compared in Fig. 2 (a) to observe the magnetic influence of the two cubic phases in S2 sample. Between 1.5 and 60 K and at very low field (B = 0.03 T) the magnetization curves $M_B(T)$ of both samples display a sharp peak with a maximum at 38(1) K (Fig. 2(a)). This comparison shows that this low temperature peak can be considered as an intrinsic property of the monoclinic deuteride. The decrease of M_B below 38 K is ascribed to the ferrimagnetic behavior features by a reinforcement of the Er magnetic moment upon cooling, thus leading to a reduced magnetization. Above 38 K the sharp decrease of M_B is attributed to the ferro to antiferromagnetic coupling of the Fe sublattice as observed for $YFe_2D_{4.2}$ and related compounds [14].

Isofield magnetization measurements were recorded at different temperatures in applied field up to 9 T (Fig. 2(b)). The pronounced magnetization peak is clearly observed in field ranging from 0.03 to 1.5 T. In this field range, the compound exhibits a ferrimagnetic type behavior. For larger applied fields, the low temperature shows a broad feature and evolves towards a ferromagnetic like behavior at 8 and 9 T (Fig. 2(b)). The main magnetic variation at 9 T is a decrease of $M_B(T)$ around 75 K.

The two studied $Y_{0.5}Er_{0.5}Fe_2D_{4.2}$ samples present very similar magnetic behavior including same transition temperatures. Consequently, the low temperature behavior is unambiguously ascribed to the monoclinic phase. The magnetic contribution of the minority cubic phases is only observable above 55K and yields higher magnetization value but no clear additional transitions. $M_T(B)$ values measured under 9 T for the two samples differs from 5 % only below 80 K.

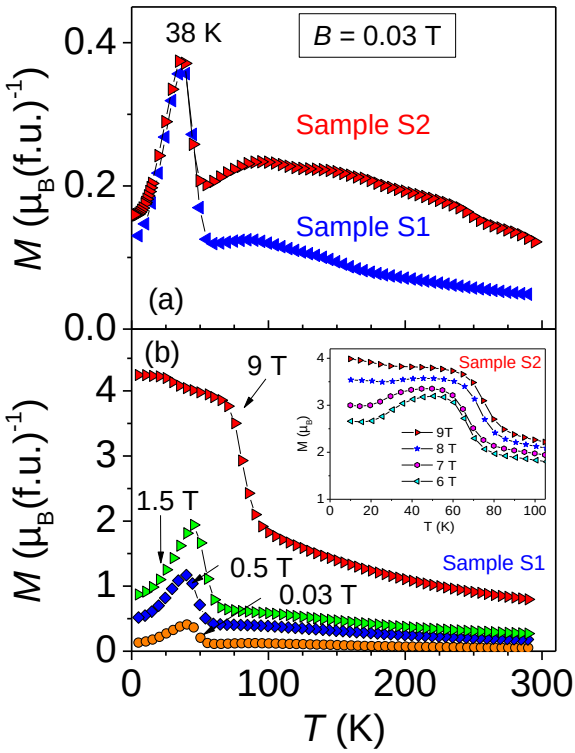

Fig. 2 : Thermomagnetization curves of the $Y_{0.5}Er_{0.5}FeD_4$ samples under different applied magnetic fields: a) comparison of S1 and S2 under 0.03T; b) Evolution of the magnetization curves under different applied field for sample S1 in main part and sample S2 in Inset.

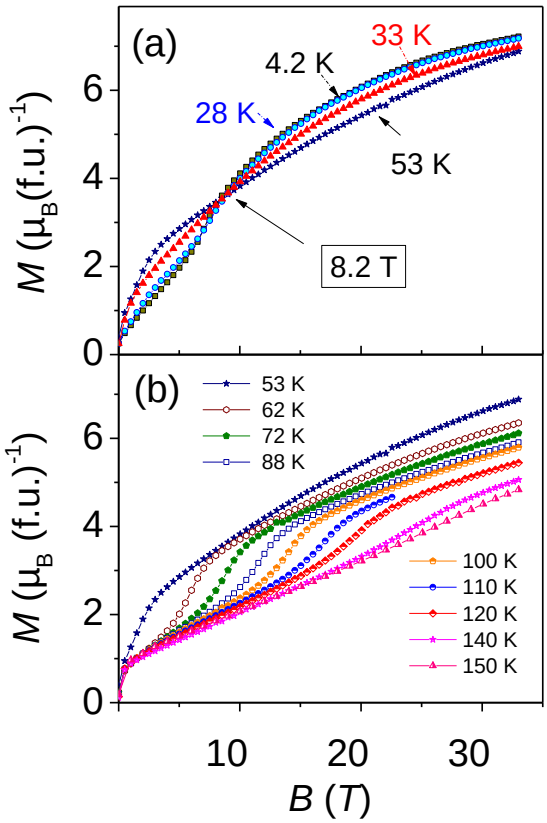

Fig. 3: Magnetization curves of the $Y_{0.5}Er_{0.5}Fe_2D_{4.0}$ compound (S2) under high magnetic field up to 35 T between 4.2 and 53 K (a) and 53K to 150 K (b).

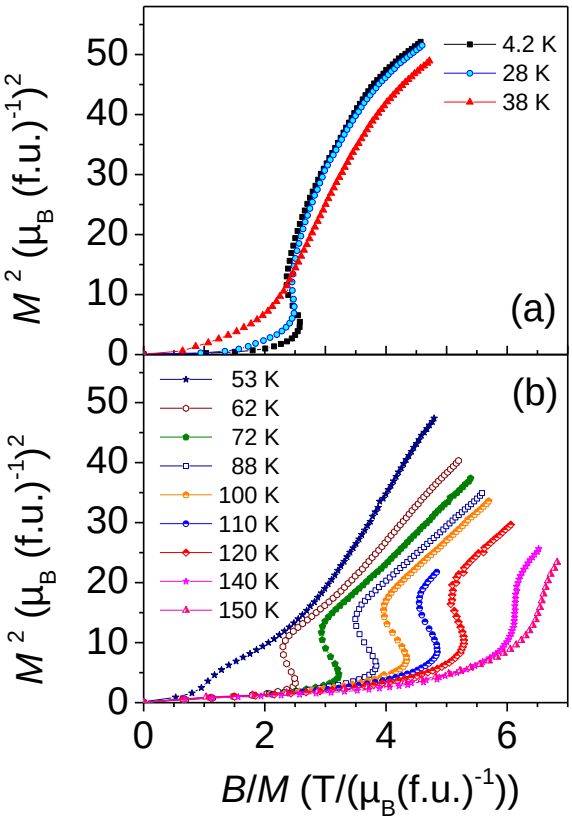

Fig. 4: Arrott-Belov curves of the $Y_{0.5}Er_{0.5}Fe_2D_{4.0}$ S2 compound measured under high magnetic field (35 T) between 4.2 and 38 K (a) and 53 K to 150 K (b).

The magnetization curves $M_T(B)$ of sample S2 recorded up to 35 T applied field are displayed in Fig. 3 for temperatures ranging between 4.2 and 150 K. The $M_T(B)$ curves between 4.2 and 53 K cross near B_{Cross}= 8.2 T with $M_B(T)$ = 3.65(5) μ_B (Fig. 3(a)). Interestingly, B_{Cross} does not change versus temperature between 4.2 and 53 K and $M_B(T)$ is close to the value measured for $YFe_2D_{4.2}$ at 4.2 K (3.76 μ_B).

Between 62 and 150 K, the $M_T(B)$ curves present a metamagnetic behavior with a critical field shifted to larger values as T increases (Fig. 3(b)). The S shape of the corresponding Arrott-Below plots (Fig. 4) clearly indicates the first order character of both metamagnetic transitions occurring for $T \leq 28$ K and $62 \leq T \leq 140$ K respectively. The intermediate behavior observed at 38 and 53 K, also leads to cross the other curves at the critical field of c.a. 8.2T. In this temperature range the transition, if any, is no longer of first order since the S shape has disappeared in the Arrott-Below plots.

The transition fields B_{Trans} are obtained at each temperature from the maximum of the $dM_T(B)/dB$ derivative and are compared to that of $YFe_2D_{4.2}$ deuteride in Fig. 5. Below 38 K,

B_{Trans} varies between 7 and 8.2 T for the Er containing compound. In this low temperature range, the Er and Fe sublattices form a ferrimagnet in the ground state. Increasing the field is expected to favor a ferromagnetic arrangement; therefore B_{Trans} is assigned to such ferri to ferromagnetic transition. The occurrence of similar metamagnetic transition from ferrimagnetic towards a ferromagnetic state has been also reported in $Y_{0.7}Er_{0.3}Fe_2D_{4.2}$ [9] .

Then above the temperature T_{M0}=38 K, B_{trans} increases linearly versus temperature for the two compounds (x=0 and 0.5); T_{M0} values being obtained by an extrapolation of B_{trans} to zero field. Note that T_{M0} also corresponds to the maximum of the peak observed in the magnetization curve of $Y_{0.5}Er_{0.5}FeD_{4.0}$ at 0.03 T. T_{M0} decreases versus the Er content and the dB_{trans}/dT slope is larger for the Er containing compound (0.24±0.01 $T.K^{-1}$) than without Er (0.15 $T.K^{-1}$). In this temperature range B_{trans} has been attributed to the transition from an AFM towards a FM state [9] through an itinerant metamagnetic behavior of the Fe sublattice.

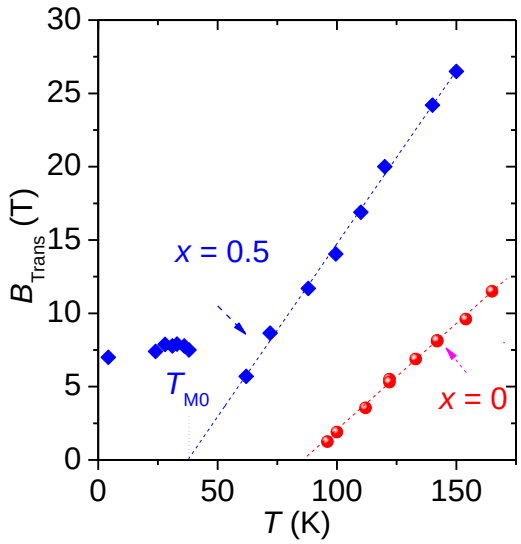

Fig. 5: Transition field B_{Trans} versus temperature for $Y_{1-x}Er_xFeD_{4.2}$ compounds (x=0, 0.5).

The spontaneous magnetization (M_{Spont}) was obtained by extrapolation of the linear part of the magnetization (above 1 T and below B_{Trans}) as defined below and in ref [9]:

$$M_T(B) = M_{Spont}(T) + \chi(T).B \qquad (1)$$

The evolution of M_{Spont} is displayed in Fig. 6(a) and is compared with that of $YFe_2D_{4.2}$.

At 4.2 K, M_{Spont}= 0.35 μ_B corresponds to $2.m_{Fe}$-$0.5.m_{Er}$ with m_{Fe}= 1.82 μ_B (Fe atom)$^{-1}$ and m_{Er}=6.58 μ_B (Er atom)$^{-1}$ assuming a collinear and antiparallel alignment of the Fe and Er

moments. The mean Fe moment m_{Fe} was assumed to be the same than for $YFe_2D_{4.2}$ and it corresponds to half the magnetization obtained at B_{Cross}. The mean Er moment m_{Er} is smaller than the free ion value (9 μ_B), but close to the value observed in $Y_{0.7}Er_{0.3}Fe_2D_{4.2}$ (m_{Er} = 6.4 μ_B (Er atom)$^{-1}$). The reduction of m_{Er} compared to the free ion value can be attributed to a strong crystal field effect related to the Er environment. The increase of M_{Spont} up to 40 K can be related to the decrease of m_{Er}. Above T_{M0}, M_{Spont} is barely identical to the value obtained for $YFe_2D_{4.2}$. We conclude that, in this high temperature range, the Fe magnetic moments are in the same magnetic state for both compounds and that the Er contribution to the magnetization is very small.

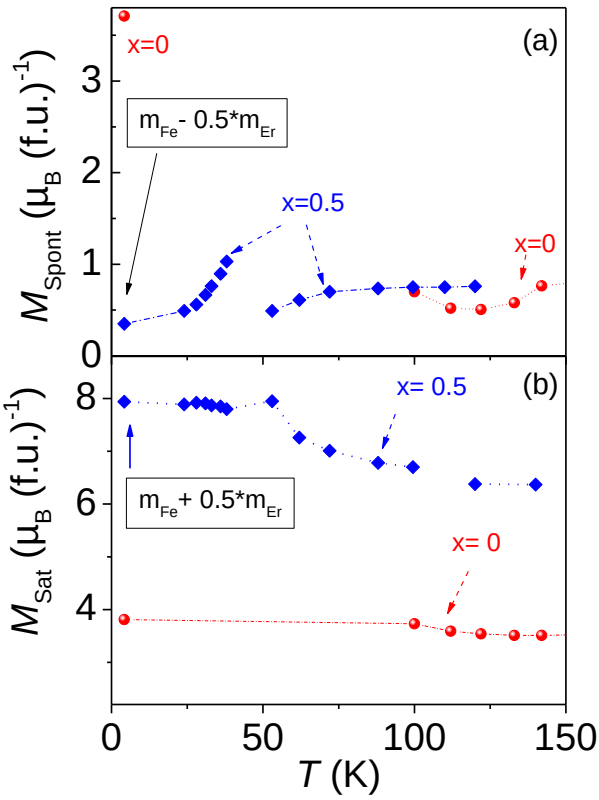

Fig. 6: Temperature evolution of the spontaneous magnetization M_{Spont} (a) and of the saturation magnetization M_{Sat} (b) for the $Y_{1-x}Er_xFeD_{4.2}$ deuterides (x=0, 0.5).

The saturation magnetization (M_{Sat}) has been extrapolated at high field using the $1/B^2$ ferromagnetic approach law above 15 T:

$$M_T(B) = M_{Sat}(T)(1 - b_M/B^2) \qquad (2)$$

M_{Sat} of $Y_{0.5}Er_{0.5}Fe_2D_{4.2}$ is significantly larger than that of $YFe_2D_{4.2}$ in all the temperature range. Assuming that the difference between the two deuterides is related to the Er moments parallel to the Fe ones, m_{Er}= 8.3 μ_B (Er atom)$^{-1}$ at 4.2 K. This value is larger than that estimated at low field but remains smaller than the Er free ion value. The observation of the $M_T(B)$ curves in Fig. 3(a) shows that the saturation is still not reached at 35 T due to the large Er anisotropy indicating that a higher magnetic field will be necessary to reach a saturated ferromagnetic state. M_{sat} is almost constant up to 53 K, then a progressive decrease is observed. The saturation magnetization of $YFe_2D_{4.2}$ is large (close to 4μ_B/f.u.) and corresponds to the field induced ferromagnetic coupling of the Fe magnetic moments. The larger value of M_{Sat} of $Y_{0.5}Er_{0.5}Fe_2D_{4.2}$ as compared to that of $YFe_2D_{4.2}$ indicates that an Er moment component parallel to the Fe magnetization should be induced by the applied magnetic field thus contributing to the total magnetization. Up to 50K, M_{Sat} of $Y_{0.5}Er_{0.5}Fe_2D_{4.2}$ remains constant at about 8μ_B/f.u. in spite of the temperature increase. Then above 50K, as can be seen from Fig. 6(b), the M_{Sat} of $Y_{0.5}Er_{0.5}Fe_2D_{4.2}$ and $YFe_2D_{4.2}$ present different behaviors. The first compound exhibits a M_{Sat} decrease versus temperature whereas for the second one, featuring the Fe sublattice only, M_{Sat} remains almost constant. The M_{Sat} difference is consequently attributed to the Er sublattice magnetization and its temperature dependence reflects the Er moment decrease versus temperature. At 150K, we estimate the field induced ferromagnetic component of the Er moment to 5.7μ_B/Er atom against 1.75μ_B/Fe atom.

Interestingly, one can notice that M_{Spont} slightly increases versus temperature whereas M_{Sat} decreases above 50 K for Er containing compound. In spite of these opposite evolutions both reflect the same thermally activated reduction of the Er magnetic moment in the ferri (or AFM) and field-induced ferromagnetic regime respectively.

3.2.2 Neutron diffraction

3.2.2.1 Magnetic structures at B=0 T

The temperature dependence of the NPD patterns measured from 2 to 300 K on D1B spectrometer is presented as a 3D plot in Fig. 7. This plot shows the existence of magnetic peaks related to three magnetic ranges: a ferrimagnetic structure at low temperature, an intermediate AFM structure between T_{M0} and T_N and a paramagnetic state above T_N. NPD patterns representative of each magnetic range (T= 2, 75 and 208 K) are displayed in Fig. 8.

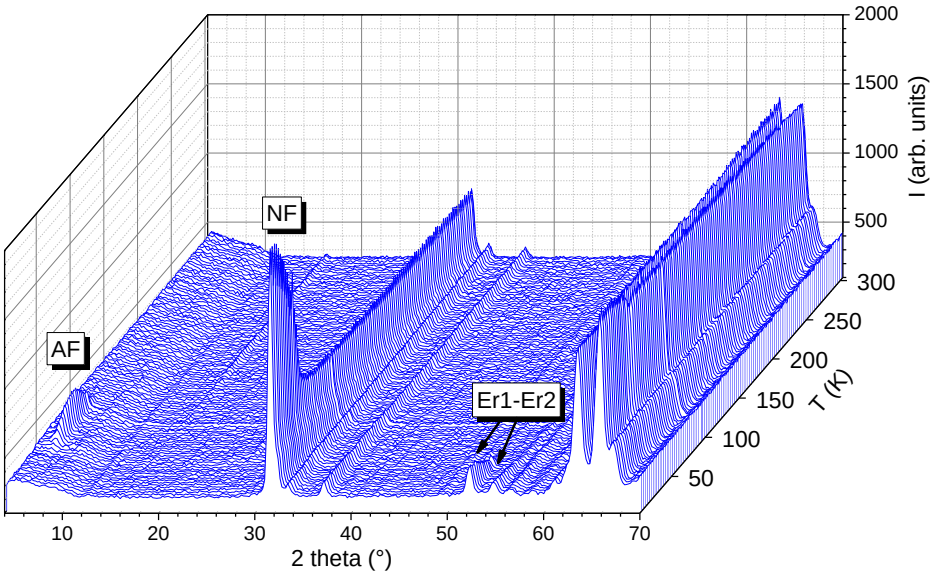

Fig. 7: Temperature evolution of the NPD patterns of $Y_{0.5}Er_{0.5}Fe_2D_{4.2}$ (sample S2) recorded every 3 K between 2 and 300 K, as measured on the *D1B* diffractometer (λ= 2.52 Å).

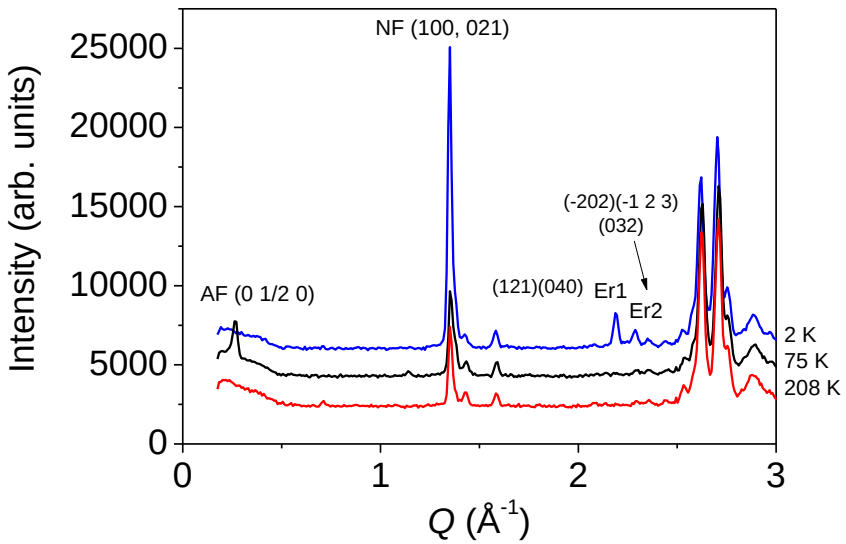

Fig. 8: NPD patterns of $Y_{0.5}Er_{0.5}Fe_2D_{4.2}$ (sample S2) at *T*=2, 75 and 208 K measured on *D1B* ($Q = 4\pi \sin\theta/\lambda$; λ= 2.52 Å).

A 2 K, three main magnetic peaks are observed: an intense peak (noted NF) at Q = 1.35 Å^{-1}, which contains the nuclear and the magnetic contributions of both Er and Fe moments, and two small peaks labelled Er1 and Er2 at Q = 2.195 and 2.296 Å^{-1} respectively, which are only due to the Er magnetic moments. The magnetic peak indexation are reported in Fig. 8. At 75 K, we observe a large peak at Q = 0.26 Å^{-1} (referred to as AF) and a smaller one at Q = 1.14 Å^{-1} which both belong to the AFM structure, whereas the intensity of the large NF peak has decreased, and the two magnetic Er1 and Er2 peaks are no more visible. Then at 208 K, only peaks belonging to the crystal structure are seeable.

In Fig. 9, the thermal variation of the intensity of the three main magnetic peaks (NF, Er1 and AF), allows to determine the magnetic ordering temperatures: the Er sublattice orders at T_{ER}=50 K, the AFM structure appears at T_{AF}=40K (close to T_{M0}= 38 K) and disappears at T_N=115 K with a maximum at 74 K. As T_{Er} is higher than T_{M0}, this means that a transition occurs between a ferrimagnetic order (Ferri) towards an AFM structure between 38 and 50 K.

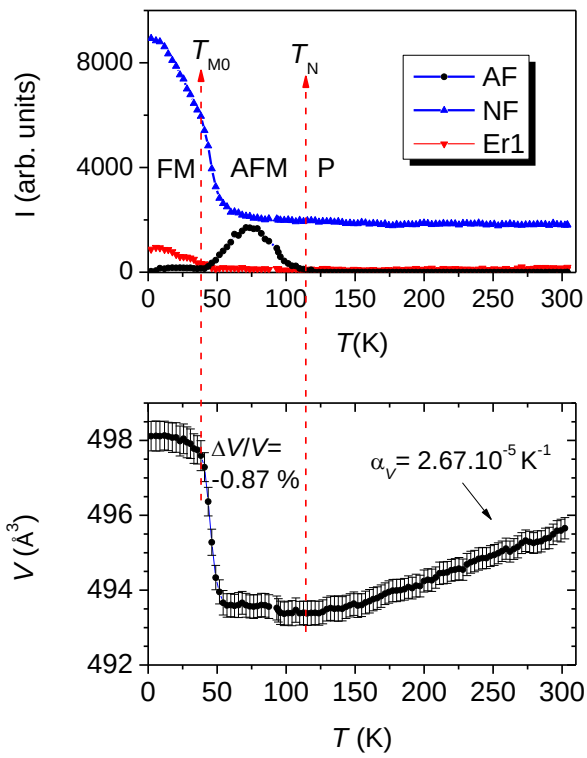

Fig. 9: Temperature dependence of (top) the intensities of AF, NF and Er1 Bragg peaks and (bottom) cell volume of $Y_{0.5}Er_{0.5}Fe_2D_{4.2}$ in zero applied field for the S2 sample. T_{M0} and T_N positions are marked with dotted line as guide for eyes.

The cell volume (bottom of Fig. 9) decreases sharply ($\Delta V/V$= -0.87 %) between 38 and 55 K with an inflexion point at 45 K, then is almost constant in the AFM range between 55 and 115 K. The linear increase of the cell volume above 115 K- in the paramagnetic range- is related to the thermal expansion with a coefficient $\alpha_V=1/V_0\ dV/dT$= 2.67(4)10^{-5} K^{-1} and V_0= 493.38Å^3. All three *a*, *b*, *c* parameters show a sharp decrease above T_{M0} (Fig. 10), with relative contractions of -0.33 % for *a*, -0.26 % for *b* and -0.31% for *c*. There is a very small variation of the monoclinic angle β near T_{M0} indicating that the monoclinic distortion is not changed. This cell parameter contraction has been attributed to the magnetostrictive effect related to the Ferri-AFM transition. In $Y_{0.7}Er_{0.3}Fe_2D_{4.2}$ the cell contraction was much more pronounced in the (*a*, *c*) plane compared to the monoclinic *b* parameter. The thermal expansion coefficients measured above 150 K are around 1.40±0.2 10^{-5} K^{-1} for *a* and *c* cell parameters and only 0.54 10^{-5} K^{-1} for *b* cell parameter. The smallest thermal expansion for *b* parameter results from the opposite influence of the monoclinic distortion and the thermal dilatation. Indeed, the lowering of the crystal symmetry from cubic towards the monoclinic structure induces a contraction of *a* and *c* cell parameters and an expansion for *b* cell parameter as *T* decreases.

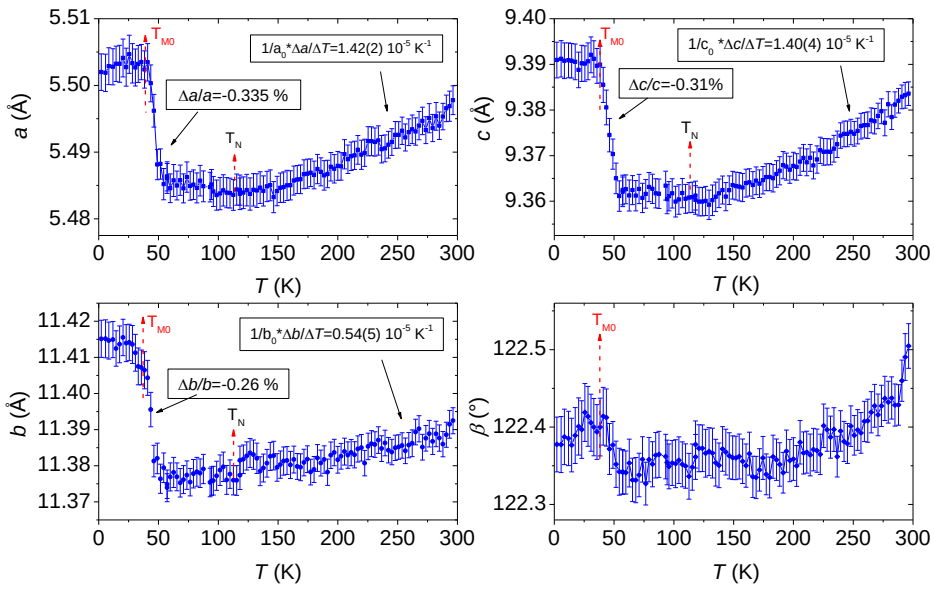

Fig 10. Cell parameters variation versus temperature. The positions of T_{M0} and T_N are indicated by arrows.

A quantitative analysis of the magnetic structure of $Y_{0.5}Er_{0.5}Fe_2D_{4.2}$ was undertaken by refining the NPD pattern measured at 10 K on 3T2. In a first attempt the NPD pattern was refined taking into account only the nuclear contribution of the three phases (one monoclinic

and two cubic phases) with the deuterium positions and occupation factors refined at 300 K and a collinear ferrimagnetic structure for the $Y_{0.5}Er_{0.5}Fe_2D_4$ monoclinic phase. This magnetic structure was described as in ref [9], with the same mean Er (Fe) moment m_{Er} (m_{Fe}) for all Er (Fe) atoms. The refined Er and Fe moments were respectively m_{Er} =7.53[15] μ_B and m_{Fe}=2.51(6) μ_B, corresponding to larger values than estimated from the magnetic measurements (m_{Er}=6.58 μ_B and m_{Fe}= 1.82 μ_B). In a second step, a magnetic structure was added for the main cubic phase (*a* =7.8939 Å at 300 K and 7.8889 Å at 10 K). This allows to obtain m_{Er}=6.43(15) μ_B and m_{Fe}=1.92(6) μ_B for the main monoclinic phase, values similar to those deduced from magnetic measurements. However, attempt to determine the magnetic structure of the cubic phase $Y_{0.5}Er_{0.5}Fe_2D_{3.2}$ assuming also a collinear ferrimagnetic structure did not permit to get precisely the Er and Fe moments in such secondary phases. Adding a magnetic contribution to the second cubic phase $Y_{0.5}Er_{0.5}Fe_2D_{1.6}$ did not improve the NPD pattern refinement nor modify the results for the monoclinic magnetic structure. Two main reasons for this being the low content of the secondary phases and the already large number of refined parameters. In addition, for the same reasons, it was not possible to perform a quantitative analysis of the antiferromagnetic structure using the NPD pattern measured at 75 K on D1B which has a limited *Q* range (0.5-3 $Å^{-1}$). Nevertheless, as $Y_{0.5}Er_{0.5}Fe_2D_{4.0}$ is isostructural to $Y_{0.7}Er_{0.3}Fe_2D_{4.0}$ and the low temperature diffraction patterns present similar magnetic peaks, it is also reasonable to assume similar collinear ferrimagnetic and antiferromagnetic structures for this compound.

3.2.2.2 Neutron diffraction experiments versus applied field

The evolution of the NPD patterns at 2 K was measured between 0 and 12 T. The main observations are a field-induced decrease of the NF line intensity and a variation of the Er1 and Er2 intensities. A plot of selected patterns between 0 and 12 T is shown in Fig. 11, whereas the variation of the NF and Er1 peak intensities versus field is displayed in Fig. 12(a). The main NF peak decreases continuously versus field with an inflexion point at 7.4 T, i.e. close to the transition field determined with the magnetization curve at 4.2 K (B_{Trans}= 7 T). The Er1 peak intensity decreases down to a minima at 6 T and increases after. The variation of the Er2 peak intensity is more difficult to observe due to its weaker intensity leading to a low signal/noise ratio). A small peak intensity decrease is however observed as the field varies from 0 to 3T, but then the intensity remains constant within the error bars. These results can be interpreted, through appropriate simulations, to a decrease of the mean Er moment magnitude, but not to a full demagnetization which would imply the disappearance of the Er1 and Er2 peaks. On the other hand, if the ferri-ferromagnetic transition was only due to a rotation of the Er moment,

the intensity of the Er2 peak should increase when that of Er1 decrease, which is not the case. It is also important to notice, that there is no significant variation of the Bragg peak position, meaning that the cell volume do not varies under applied field.

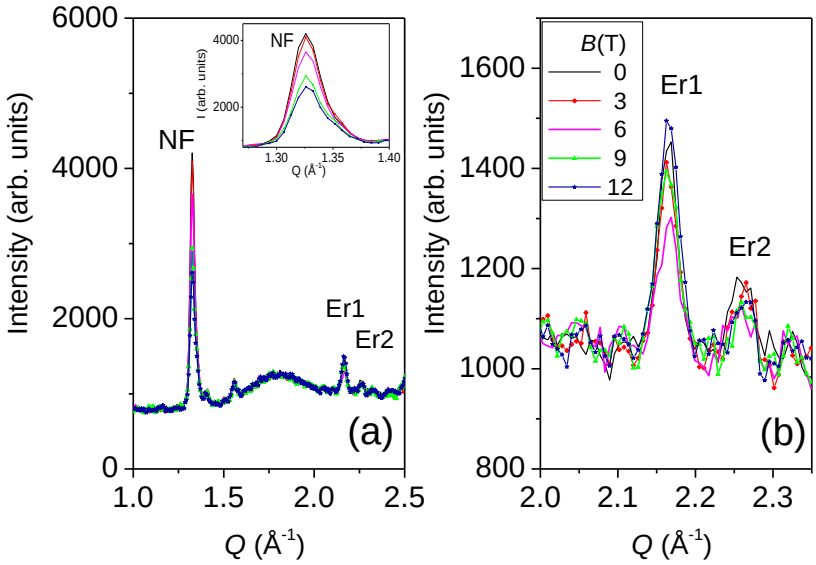

Fig. 11. Neutron powder diffraction patterns of $Y_{0.5}Er_{0.5}Fe_2D_{4.2}$ recorded at 2 K under various magnetic fields on the E6 (BENSC) spectrometer (λ = 2.454 Å). Inset (a) zoom on NF peak. (b) zoom on Er1 and Er2 peaks.

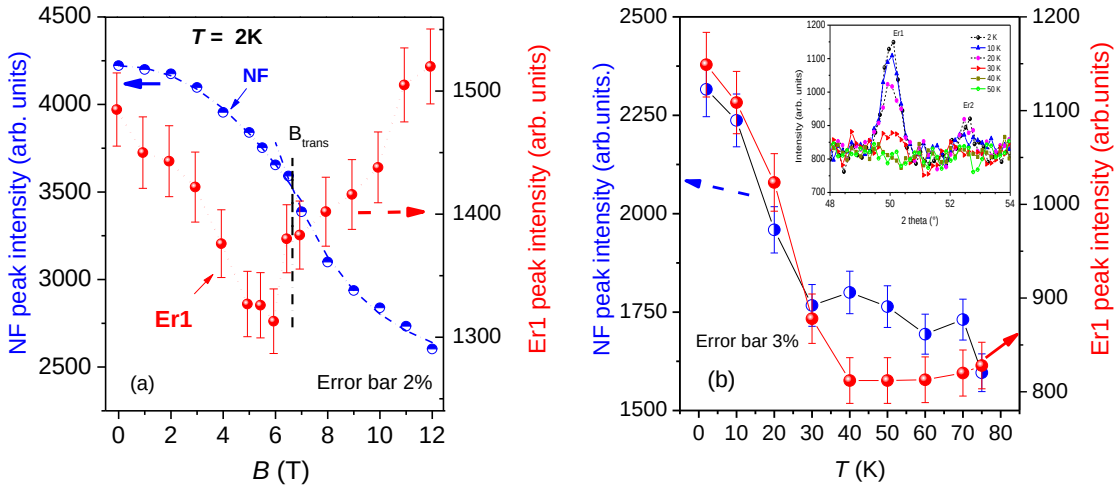

Fig 12: Variations of the NF and Er1 peak intensities of the $Y_{0.5}Er_{0.5}Fe_2D_{4.2}$ deuteride versus applied magnetic field at 2K (a) and versus temperature under 10 T (b). The inset of Fig 12(a) corresponds to a zoom on Er1 and Er2 peaks at selected temperatures.

The evolution of the NF and Er1 peak intensity at 10 T versus temperature is similar (Fig. 12(b)), with a progressive intensity decrease reaching a constant value above 40 K. It can be attributed to the reduction of the Er magnetic moment, as already observed at zero field.

The NPD patterns were measured versus applied field at T= 50, 55, 65 and 75 K, i.e. above T_{M0}=38 K. The variation of the NF peak intensity is presented in Fig. 13 (top). At low field, the compound is antiferromagnetic as a weak AF peak is observed in the patterns. At 75 K, were this AF peak is more visible, a smooth decrease of its intensity is observed between 0 and 6 T. The transition is therefore characterized by simultaneous variation of two Bragg peak intensities versus field: a decrease of the AF peak and an increase of the NF peak. Additionally, the magnetic field which triggers the increase of the NF Bragg peak intensity is shifted to higher values upon increasing temperature (see Fig. 13). These shifts are in agreement with B_{trans} variation versus *T*, as observed in the magnetization curves (Fig. 5). This clearly confirms that this metamagnetic transition corresponds to the AFM-FM transition. Therefore, the progressive NF peak intensity change at B_{Trans} can be attributed to both the rotation of half of the Fe magnetic moments (from AFM to FM) and a contribution of a field-induced Er magnetic moment component parallel to the Fe moments. This change of the Er moment results from the field experienced at the Er position which is the sum of the applied magnetic field and the molecular field produced by the Fe sublattice in the ferromagnetic state.

In addition, the expansion of the interplanar distances of the NF peak (d_{NF}) is observed as the magnetic field increases follows the NF intensity variation (Fig. 13). It confirms the existence of a magnetostrictive effect at the AFM-FM transition as previously observed for $YFe_2D_{4.2}$ and $Y_{0.7}Er_{0.3}Fe_2D_{4.2}$ [9, 16]. The relative distance variation $\Delta d_{NF}/d_{NF}$ = 0.35 % is comparable to the thermal contraction observed for the *a* cell parameter (0.31 %). As the NF peak is indexed with (100) miller indices, this indicated that the magnetostrictive effect induced either by temperature or applied field is of the same order of magnitude.

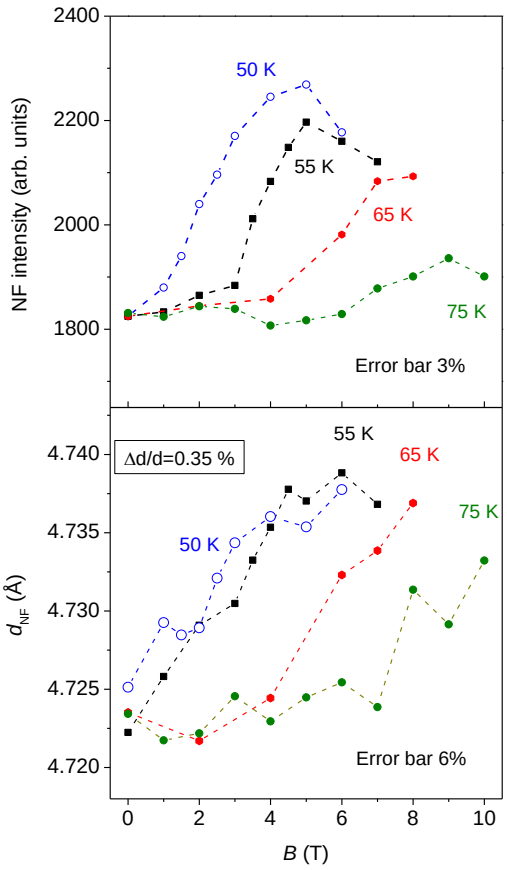

Fig. 13: Evolution of the NF peak intensity (top) and of the interplanar d_{NF} distance (bottom) for $Y_{0.5}Er_{0.5}Fe_2D_{4.2}$ deuteride at 50, 55, 65 and 75 K.

4. Discussion

This study has shown the existence of two different types of metamagnetic transitions in $Y_{0.5}Er_{0.5}Fe_2D_4$: the first one at low temperature which is observed only for Er containing compounds and the second one observed in all $Y_{1-x}Er_xFe_2D_{4.2}$ compounds including x=0. Both transitions present a first order character but have different physical origin, and therefore will be discussed separately below. It will then be followed by a more general conclusion.

4.1 Low temperature metamagnetic transition ($T \leq 38K$)

In the ground state and below 38 K, the Er and Fe sublattices form a ferrimagnetic structure. A metamagnetic transition occurs at a transition field B_{trans}= 7.5±0.5 T, which remains

almost constant between 4.2 and 38 K. This transition has been related to a change from a ferrimagnetic towards a ferromagnetic structure, i.e. from an antiparallel towards a parallel alignment of both Er and Fe moments. At low field the mean Er moment is 6.4 μ_B/Er atom only, its reduction compared to the Er^{3+} free ion value can be attributed to a crystal field effect. At high magnetic field the Er moment becomes larger (m_{Er}=8.3 μ_B (Er atom)$^{-1}$). This ferri-ferromagnetic transition originates from the application of a magnetic field surpassing the Er-Fe interaction, and occurs at a relatively low field (7.5 (5) T) compared to other compounds in the literature. Indeed, in heavy rare-earth containing RE_2TM_{17} compounds the transition fields required to induce a ferromagnetic alignment ranges between 40-50 T [5, 6, 17]. Hydrogen absorption yields an increase of the interatomic distances between the Er and Fe atoms and therefore a decrease of the strength of the Er-Fe exchange interaction. According to Tereshina et al. [7], the reduced exchange integral $J_{RE\text{-}Fe}(y)/J_{RE\text{-}Fe}(0)$ decreased linearly with the relative cell volume ($\Delta V/V$) and a larger reduction was found in REFe$_2$ hydrides (RE=Tm, Er, Ho) compared to those of RE_2Fe$_{17}$ hydrides, as they absorb larger H/RE hydrogen content. For example in $Tm_2Fe_{17}H_y$, the transition from ferrimagnetic to ferromagnetic state at 4.2 K occurs between 30 and 57 T, [6, 7] whereas in the corresponding alloy the magnetization increases in four steps and the saturation is not reached at 74 T [6]. In rhombohedral $TmFe_2H_{3.4}$, B_{Trans} was only 10 T at 4.2 K and the ferromagnetic state was reached at 100 T, due to a strong anisotropy of the Tm sublattice [8]. The cell volume of $Tm_2Fe_{17}H_y$ decreases of only 4.2 %, and that of $TmFe_2H_{3.4}$ of 24.1 %. Consequently, the reduction of the molecular field coefficient can be estimated to be 20 % in $Tm_2Fe_{17}H_y$ and 62 % in $TmFe_2H_{3.4}$. As in $Y_{0.5}Er_{0.5}Fe_2D_{4.2}$, the cell volume increase reaches 26.7 %, a large reduction of the $J_{Er\text{-}Fe}$ exchange interaction is therefore expected. Interestingly this transition field observed in $Y_{0.5}Er_{0.5}Fe_2D_{4.2}$ is not very sensitive to the Er content as it remains close to that observed in $Y_{0.7}Er_{0.3}Fe_2D_{4.2}$.

The transition from the ferrimagnetic to ferromagnetic state can occur through different ways: a demagnetization of the RE moments as proposed in [4, 6] or a rotation with constant magnetic moment magnitude [18]. The $M_T(B)$ curves of $Y_{0.5}Er_{0.5}Fe_2D_{4.1}$ cross at a value corresponding to 2.m_{Fe} suggesting a demagnetization of the Er sublattice with a minimum around 8 T. In addition, the previous NPD results in $Y_{0.7}Er_{0.3}Fe_2D_{4.1}$ isotype, have suggested a demagnetization process of the Er moment, but the Er1 and Er2 peak intensities were small and it was difficult to fully conclude owing the low signal/noise ratio [9].

In the present study, the variation of Er1 contribution versus applied field is more clearly seen in the NPD patterns thanks to its larger Er content. All the NPD patterns measured at 2 K

indicates the absence of additional Bragg peaks and shows a field dependence of the NF and Er1 peak intensities (Figs. 11-12). The field evolution of the NPD patterns reveals a progressive decrease of the Er contribution down to about 6 T and an increase above with an Er moment parallel to that of Fe as confirmed by magnetic measurements. Although the Er demagnetization is not complete at B_{trans} - there is still an Er contribution in the NPD patterns – this Ferri-Ferro transition occurs through a possible reduction of the Er moment.

4.2 High temperature metamagnetic transition (T>38K)

The NPD pattern analysis at zero field, indicates that the Er sublattice orders below T_{Er} = 50 K (Figs 9 and 12) whereas the AF line appears above 40 K, which means that there is a small temperature range were the ferrimagnetic structure (Er moments coupled antiparallel to all Fe moments) coexists with the antiferromagnetic structure (AFM dominated by the Fe magnetic moments). The metamagnetic behavior observed above T_{M0}= 38 K, corresponds therefore to a transition from an AFM to a FM state.

According to previous studies on $YFe_2D_{4.2}$ (x=0) this transition is related to the IEM behavior of the Fe sublattice. In these previous works [9, 16], the AFM structure has been described as the alternance of two ferromagnetic layers with Fe moments perpendicular to the monoclinic ***b*** axis and in opposite direction to each other, separated by a row of non-magnetic Fe atoms. As in the monoclinic cell there are 8 different Fe sites with different number of neighboring H atoms, it was shown that one Fe atom which is surrounded by 4.7 D neighbor atoms loses its magnetic moment at T_{M0} and form a nonmagnetic Fe row perpendicular to the ***b*** axis. Such non-magnetic Fe atoms are found to be located at the Fe7 position (Table 2). Then the shortest Fe-Fe distance between the 6 Fe atoms surrounding the Fe7 atoms becomes larger (> 4.7Å) and the coupling between their magnetic moments negative. Similar Fe sublattice behavior is therefore expected in the case of $Y_{0.5}Er_{0.5}Fe_2D_{4.2}$. The remaining question is then how the Er moments behaves at this AFM-FM transition. At low field the spontaneous magnetization above T_{M0} is very close for $Y_{0.5}Er_{0.5}Fe_2D_{4.2}$ and $YFe_2D_{4.2}$ which suggests that the Er moments do not contribute to the magnetization. Additionally no Er peaks are observed in the NPD pattern in the AFM range, indicating that the Er moment are not ordered in the AFM structure.

In $Y_{0.5}Er_{0.5}Fe_2D_{4.2}$ the IEM transition field B_{Trans} increases linearly versus the temperature up to 150 K, with a slope dB/dT =0.24±0.01 $T.K^{-1}$. Similar linear increase of B_{Trans}

has also been observed in $Hf_{0.825}Ta_{0.175}Fe_2$ Laves phase which displays also an FM-AFM transition with T_{M0}= 195±0.05 K and d*B*/d*T* =0.13±0.01 T.K^{-1} [19, 20].

For temperatures close to T_{M0} the Ferri-AFM transition is abrupt and is accompanied by a cell volume increase. When *T* increases, the change of magnetic order occurs in a broader range of temperature. According to NPD studies on $Y_{0.5}Er_{0.5}Fe_2D_{4.2}$, the Néel temperature at zero applied field is T_N =115 K, but metamagnetic behavior is still observed up to 150 K, indicating that paramagnetic-ferromagnetic transitions are taking place above T_N (Figs. 3 and 4).

The shape of the magnetization curves indicates that the ferromagnetic state is not fully reached at 35 T, but that a field-induced component of the Er magnetic moment aligned parallel to the Fe sublattice should be considered to explain the evolution of the saturation magnetization. Above B_{trans} the combination of the molecular field and the applied magnetic field should be sufficient to induce an Er moment parallel to the Fe moments.

Another feature of this metamagnetic transition is the sensitivity of T_{M0} to the cell volume variation upon Er for Y substitution. Indeed, taking into account previous results on $Y_{0.7}Er_{0.3}Fe_2D_{4.2}$, T_{M0} decrease versus the cell volume of the deuterides with a slope dT_{M0}/dV= 7.7 K Å^{-1}. This Er/Y substitution effect is comparable in magnitude but smaller than the 12.7 K Å^{-1} value reported for $YFe_2(H,D)_{4.2}$ compounds [14] where the cell volume increase linearly upon H for D substitution. The influence of the applied pressure on T_{M0} was examined for $YFe_2D_{4.2}$ and $YFe_2H_{4.2}$ [21, 22]. Different dT_{M0}/dV slopes were obtained for the deuteride and the hydride, but they converged towards a critical volume V_C= 501.7 Å^3, below which the ferromagnetic ground state was suppressed. The stabilization of an AFM ground state by applying an external pressure of few tent of GPa has been observed in other Fe rich compounds like RE_2Fe_{17} compounds (*RE*= Y, Lu and Ce) [23, 24]. Er for Y substitution in $YFe_2D_{4.2}$ can be considered as a chemical pressure effect, and it can be expected that the ferrimagnetic state will be suppressed for larger Er content. Nevertheless, the critical cell volume should be lower than for $YFe_2(H,D)_{4.2}$ under pressure, as the cell volume of $Y_{0.5}Er_{0.5}Fe_2D_{4.2}$ (V=496.6(3) Å^3) is already smaller than V_C and a linear extrapolation of T_{M0}=f(V) yields 492 Å^3 . This means that the influence of Er for Y substitution on T_{M0} in not a pure chemical pressure effect, and that the magnetic contribution of Er influence also the stability of the ferrimagnetic state.

Such relationship between magnetic ordering temperature and unit cell volume has been observed in other systems presenting IEM effect, like in $La(Fe,Si)_{13}H_y$ [25, 26] compounds.

This relationship can be a consequence of a change of the density of state at the Fermi level induced by unit cell volume expansion and possible modifications of the splitting of the minority and majority band and/or the curvature of the Landau d band.

5. Conclusions

Combining magnetic field measurements with neutron powder diffraction, this experimental study on $Y_{0.5}Er_{0.5}Fe_2D_{4.2}$ has showed the existence of two different types of first order metamagnetic transitions depending on the temperature range. The first one observed at low temperature is explained by a forced ferrimagnetic to ferromagnetic transition with a field-induced reorientation of the Er moment parallel to the Fe one. The transition field is not very sensitive to the temperature, and its low value (7-8T) compared to that of other Fe rich intermetallics is attributed to the significant weakening of the Er-Fe exchange interaction due to the 27 % cell volume expansion induced by the 4 D atom f.u.$^{-1}$ insertion. This study confirms the earlier results on $Y_{0.7}Er_{0.3}Fe_2D_{4.2}$ and is in agreement with the assumption that strong reduction of the *RE*-Fe interaction occurs upon H insertion.

Then, above T_{M0}=38K, a second AFM-FM metamagnetic transition is observed for $Y_{0.5}Er_{0.5}Fe_2D_{4.2}$. This transition is related to the IEM behavior of the Fe sublattice, with a linear variation of B_{trans} versus temperature. T_{M0} and B_{trans} are very sensitive to the Er content and the significant unit cell volume change. It can be attributed to a strong magnetoelastic coupling. The cell volume contraction observed at T_{M0} confirms the itinerant character of the Fe moment. At larger applied magnetic fields (> B_{trans}), an Er moment is induced and forced to align parallel to the Fe magnetic moment.

Further studies will be performed in order to have a more systematic overview of the influence of Er content and of the (H,D) isotope effect on the magnetic properties of $Y_{1-x}Er_xFe_2(H,D)_{4.2}$ compound. It will be also planned to investigate the influence of the nature of the substituted rare-earth element on both metamagnetic transitions. Indeed the strong lowering of the *RE*-Fe interactions by a large hydrogen content insertion, will allow to study the forced ferri-ferromagnetic transitions for heavy *RE* ranging from Gd to Tm.

ACKNOWLEDGMENTS

The authors thank the Institut Laue Langevin (ILL, Grenoble, France), the Laboratoire Léon Brillouin (LLB, Saclay, France) and the Grenoble High Magnetic Field Laboratory (GHMFL, Grenoble, France), as well as the Helmholtz Zentrum Berlin (Berlin, Germany) for the allocated beam time to perform the experiments. This research project at HZB has been supported by the European Commission under the 6th Framework Program through the Key Action: Strengthening the European Research Area, Research Infrastructures. Contract n°: RII3-CT-2003-505925 (NMI3).

References

[1] G. Kido, S. Kajiwara, Y. Nakagawa, S. Hirosawa, M. Sagawa, High-field magnetization of $R_2FE_{14}B$ compounds measured up to 55-T, Ieee Transactions on Magnetics 23 (1987) 3107-3109.
[2] H. Kato, D.W. Lim, M. Yamada, Y. Nakagawa, H.A. Katori, T. Goto, Field-Induced Phase-Transitions In Ferrimagnetic $R_2Fe_{14}B$ In Ultra-High Magnetic-Fields, Physica B 211 (1995) 105-107.
[3] N.V. Kostyuchenko, A.K. Zvezdin, E.A. Tereshina, Y. Skourski, M. Doerr, H. Drulis, I.A. Pelevin, I.S. Tereshina, High-field magnetic behavior and forced-ferromagnetic state in an $ErFe_{11}TiH$ single crystal, Phys. Rev. B 92 (2015) 104423.
[4] A.V. Andreev, M.D. Kuz'min, Y. Narumi, Y. Skourski, N.V. Kudrevatykh, K. Kindo, F.R. de Boer, J. Wosnitza, High-field magnetization study of a Tm_2Co_{17} single crystal, Phys. Rev. B 81 (2010) 134429.
[5] A.V. Andreev, Y. Skourski, M.D. Kuz'min, S. Yasin, S. Zherlitsyn, R. Daou, J. Wosnitza, A. Iwasa, A. Kondo, A. Matsuo, K. Kindo, Magnetic and magnetoelastic anomalies of an Er_2Co_{17} single crystal in high magnetic fields, Phys. Rev. B 83 (2011) 184422.
[6] O. Isnard, A.V. Andreev, M.D. Kuz'min, Y. Skourski, D.I. Gorbunov, J. Wosnitza, N.V. Kudrevatykh, A. Iwasa, A. Kondo, A. Matsuo, K. Kindo, High magnetic field study of the Tm_2Fe_{17} and $Tm_2Fe_{17}D_{3.2}$ compounds, Phys. Rev. B 88 (2013) 174406.
[7] E.A. Tereshina, M.D. Kuz'min, Y. Skourski, M. Doerr, W. Iwasieczko, J. Wosnitza, I.S. Tereshina, Forced-ferromagnetic state in a $Tm_2Fe_{17}H_5$ single crystal, J. Phys.: Cond. Matter 29 (2017) 24LT01.
[8] N.V. Mushnikov, N.K. Zajkov, M.I. Bartashevich, T. Goto, H. Aruga-Katori, M. Yamaguchi, I. Yamamoto, Magnetization process and magnetic structure of the $TmFe_2H_{3.4}$ hydride in ultrahigh magnetic fields up to 100 T, J. Magn. Magn. Mat. 167 (1997) 229-236.
[9] V. Paul-Boncour, M. Guillot, O. Isnard, A. Hoser, High field induced magnetic transitions in the $Y_{0.7}Er_{0.3}Fe_2D_{4.2}$ deuteride, Phys. Rev. B 96 (2017) 104440.
[10] T. Leblond, V. Paul-Boncour, A. Percheron-Guégan, Isotope effect on the thermodynamic and structural properties of $Y_{1-y}R_yFe_2(H,D)_{x(\gamma)}$ compounds (R=Tb, Er, Lu; $4.0 < x(\gamma) \leq 4.5$), J. Alloys Compds 446-447 (2007) 419-422.
[11] M. Guillot, V. Paul-Boncour, T. Leblond, Magnetic properties of $Y_{0.7}Er_{0.3}Fe_2(H,D)_{4.2}$ compounds under continuous magnetic field up to 35 tesla., J. Appl. Phys. 107 (2010) 09E144.

[12] J. Rodríguez-Carvajal, FULLPROF: A Program for Rietveld Refinment and Pattern Matching Analysis, Abstract of the Satellite Meeting on Powder Diffraction of the XVth Congress of the International Union of Crystallography, Toulouse, France, 1990, pp. 127.
[13] J. Ropka, R. Cerny, V. Paul-Boncour, T. Proffen, Deuterium ordering in Laves phases deuterides $YFe_2D_{4.2}$, J. Solid State Chem. 182 (2009) 1907-1912.
[14] V. Paul-Boncour, M. Guillot, G. Wiesinger, G. André, Giant isotopic effect on the itinerant electron metamagnetism in $YFe_2(H_yD_{1-y})_{4.2}$, Phys. Rev. B 72 (2005) 174430.
[15] V. Paul-Boncour, A. Lindbaum, E. Gratz, E. Leroy, A.S.-.-. Percheron-Guégan, Structural study of the pseudobinary $Y(Ni,Cu)_2$ system, Intermetallics 10 (2002) 1011-1017.
[16] V. Paul-Boncour, M. Guillot, O. Isnard, B. Ouladdiaf, A. Hoser, T. Hansen, N. Stuesser, Interplay between crystal and magnetic structures in $YFe_2(H_\alpha D_{1-\alpha})_{4.2}$ compounds studied by neutron diffraction, J. Solid State Chem. 245 (2017) 98-109.
[17] O. Isnard, A.V. Andreev, O. Heczko, Y. Skourski, High magnetic field study of the $Dy_2Fe_{17}H_x$ compounds with x=0–3.8, J. Alloys Compds 627 (2015) 101-107.
[18] O. Isnard, Y. Skourski, L.V.B. Diop, Z. Arnold, A.V. Andreev, J. Wostnitza, A. Iwasa, A. Kondo, A. Matsuo, K. Kindo, High magnetic field study of the Gd-Co exchange interactions in $GdCo_{12}B_6$, J. Appl. Phys. 11 (2012) 093916.
[19] L.V.B. Diop, M. Amara, O. Isnard, Large magnetovolume effects due to transition from ferromagnetic to antiferromagnetic state in $Hf_{0.825}Ta_{0.175}Fe_2$ intermetallic compound, J. Phys.: Condens. Matter 25 (2013) 416007.
[20] L.V.B. Diop, O. Isnard, E. Suard, D. Benea, Neutron diffraction study of the itinerant-electron metamagnetic $Hf_{0.825}Ta_{0.175}Fe_2$ compound, Solid State Comm. 229 (2016) 16-21.
[21] O. Isnard, V. Paul-Boncour, Z. Arnold, On the origin of the giant isotopic effect of hydrogen on the magnetic properties of $YFe_2A_{4.2}$ (A = H, D): A high pressure study, Appl. Phys. Lett. 102 (2013) 122408.
[22] O. Isnard, V. Paul-Boncour, Z. Arnold, C.V. Colin, T. Leblond, J. Kamarad, H. Sugiura, Pressure-induced changes in the structural and magnetic properties of $YFe_2D_{4.2}$, Phys. Rev. B 84 (2011) 094429.
[23] I. Medvedeva, Z. Arnold, A. Kuchin, J. Kamarad, High pressure effect on magnetic properties and volume anomalies of Ce_2Fe_{17}, J. Appl. Phys. 86 (1999) 6295-6300.
[24] J. Kamarád, O. Prokhnenko, K. Prokeš, Z. Arnold, Magnetization and neutron diffraction studies of Lu_2Fe_{17} under high pressure, J. Phys.: Condens. Matter 17 (2005) S3069.
[25] S. Fujieda, A. Fujita, K. Fukamichi, Y. Yamazaki, Y. Iijima, Giant isotropic magnetostriction of itinerant-electron metamagnetic $La(Fe_{0.88}Si_{0.12})_{13}H_y$, Appl. Phys. Lett. 79 (2001) 653-655.
[26] A. Fujita, S. Fujieda, K. Fukamichi, Influence on hydrogenation on the electronic structure and the itinerant-electron metamagnetic transition in a strong magnetocaloric compound $La(Fe_{0.88}Si_{0.12})_{13}$, J. Magn. Magn. Mat. 321 (2009) 3553-3558.